Available online at www.sciencedirect.com
SCIENCE DIRECT®
Physics of the Earth and Planetary Interiors xxx (2004) xxx–xxx
PHYSICS OF THE EARTH AND PLANETARY INTERIORS
www.elsevier.com/locate/pepi

Thermo-chemical structure in the mantle arising from a three-component convective system and implications for geochemistry

Takashi Nakagawa [a,*], Paul J. Tackley [a,b]

[a] *Department of Earth and Space Sciences, University of California, Los Angeles, CA 90095-1567, USA*
[b] *Institute of Geophysics and Planetary Physics, University of California, Los Angeles, CA 90095-1567, USA*

Received 31 August 2002; accepted 30 May 2003

Abstract

Numerical simulations are used to characterize structures and observational signatures of thermo-chemical convection with three component of differing densities nominally corresponding to regular mantle (the depleted Mid Oceanic Ridge Basalt (MORB) source), primitive mantle and recycled crust. Strong heterogeneity, similar to that observed in seismic tomography models, is generated near the CMB by sweeping of the highest density 'recycled' component into piles by convective downwellings. Meanwhile, the medium density 'primitive' material is widely dispersed by the convection and forms 'blobs'. Two types of upwelling plumes are observed: large plumes arising from the top of dense piles and small-scale plumes arising from the base of the transition zone resembling seismic tomography images of upwelling plumes [Zhao, Earth Planet. Sci. Lett. 192 (2001) 251], although the origin of these plumes is unclear. The horizontal spectra of the seismic velocity had anomalies at different depths are most similar to tomographic models when dense basal piles are present. Comparing to geochemically-required residence times, the source of HIMU (this type of rock has high ratio of helium isotope anomaly) Ocean Island Basalt (OIB) is more likely to be dense 'piles', while lower mantle blobs have been proposed as a location of primitive material. Thus the combination of blob structures and deep mantle piles may be plausible way of simultaneously satisfying geochemical and seismological constraints on mantle structure.

Keywords: Thermo-chemical convection; CMB; Seismic anomalies; OIB reservoirs; Mantle plumes

1. Introduction

Recently, several models have been proposed to explain geochemical constraints on mantle structures while simultaneously being consistent with the structure imaged by global seismic tomography models (see Tackley (2000)). Some possibilities are: (i) a global, mostly hidden undulating layer of primitive material at a mean depth of ~1700 km (Van der Hilst and Karason, 1999; Kellogg et al., 1999; Albarede and van der Hilst, 1999); (ii) isolated "piles" of anomalous material corresponding to the "superplumes" images in seismic tomographic models (Tackley, 1998, 2002); and (iii) blobs of primitive material distributed throughout the lower mantle (Becker et al., 1999; Manga, 1996). The plausibility of these models has

* Corresponding author. Present address: Department of Geophysical Sciences, University of Chicago, 5734 S. Ellis Avenue, Chicago, IL 60637, USA. Tel.: +1-310-825-9296; fax: +1-310-825-2779.
E-mail address: takashi@ess.ucla.edu (T. Nakagawa).

0031-9201/$ – see front matter © 2004 Elsevier B.V. All rights reserved.
doi:10.1016/j.pepi.2003.05.006

not been systematically investigated using numerical models of mantle convection, but a global layer has been argued against based on the lack of seismic scattering at that depth (Vidale et al., 2001), the strong (but unobserved) seismic signature that such a layer would have based on numerical modeling (Tackley, 2002), and the difficulty in explaining Earth's thermal history with such a layer present (McNamara and van Keken, 2000).

In addition to these relatively large-scale modes of compositional heterogeneity extending at least 500 km from the core–mantle boundary (CMB), the D″ layer at the base of the mantle (see Lay et al., 1998 for a review) is strongly heterogeneous, which may indicate the presence of compositionally anomalous material restricted to 200–300 km above the CMB, although two other explanations have also been proposed, namely thermal (including partial melting) or phase transition (Sidorin and Gurnis, 1998). However, in this study it is considered that strong heterogeneity of D″ is generated, at least in part, by compositional heterogeneity, an interpretation that is consistent with mineral physics (Karato and Karki, 2001), density structure of the mantle obtained by inverting normal mode splitting of free oscillation data (Ishii and Tromp, 1999, 2001) and thermal constraints on the signature of subducted slabs at the CMB (Meriaux et al., 1998).

Geochemical constraints (e.g., Hofmann, 1997) require the presence of at least two types of compositionally-anomalous material, one with a high U/Pb ratio (HIMU), generally interpreted to be "primitive" undegassed material although a recycled explanation has been proposed (Cotice and Ricard, 1999), and one corresponding to recycled crust, i.e., the endmembers HIMU, EMI and EMII (for definition, see Hofmann (1997)). Thus, the models presented here include two chemically-anomalous components, one of which nominally represents primitive material, perhaps left over from the initial differentiation of Earth (Stevenson, 1990), and the other of which nominally represents recycled crust, perhaps segregated at the CMB (Christensen and Hoffmann, 1994; Ferrachat and Ricard, 2001; Ohtani and Maeda, 2001). However, since our model does not include trace elements these designations are only nominal, the only difference between the components being the density and amount. Thus, we refer to nominally primitive material as "P-type", and nominally recycled eclogitic crustal material as "E-type".

This paper focuses on the signature of the volumetric heterogeneity associated with two types of dense material, considering the visual patterns, and the statistical diagnostics of spectral heterogeneity map (Tackley et al., 1994) in a two-dimensional cylindrical geometry. We also discuss geochemical mantle dynamics model using our modeling in comparison with geochemical constraints.

2. Model and parameters

The model assumes a two-dimensional half-cylindrical geometry, which the surface area at each boundary is adjusted similar to a spherical geometry (cylindrical–spherical rescaling), and infinite Prandtl number and extended Boussinesq approximations, allowing depth-dependence of thermal expansivity and diffusivity. Since three-dimensional simulation including tracer particles is too expensive to carry out practical computational time, two-dimensional cylindrical shell based on the cylindrical–spherical rescaling proposed by Van Keken (2001) is one of the best option for simulating a spherical shell-like geometry. A three-component chemical composition is assumed, requiring two compositional variables. Meanings and values of the non-dimensional parameters are given in Table 1, which also includes nominal dimensional values. The standard non-dimensionalization to depth of the mantle ($r_o - r_i$), and thermal diffusion time-scale and velocity are used, leading to the following non-dimensionalized forms of the governing equations:

$$\begin{aligned}
&\left(\frac{1}{r^2}\frac{\partial^2}{\partial\theta^2} - \frac{\partial^2}{\partial r^2} - \frac{2}{r}\frac{\partial}{\partial r}\right)\\
&\quad\times\left[\eta(T,z)\left(\frac{1}{r^2}\frac{\partial^2\psi}{\partial\theta^2} - r\frac{\partial}{\partial r}\left(\frac{1}{r}\frac{\partial\psi}{\partial r}\right)\right)\right]\\
&\quad+\left(\frac{1}{r}\frac{\partial^2}{\partial r\,\partial\theta} + \frac{1}{r^2}\frac{\partial}{\partial\theta}\right)\\
&\quad\times\left[4\eta(T,z)\left(\frac{1}{r}\frac{\partial^2}{\partial r\,\partial\theta} - \frac{1}{r^2}\frac{\partial}{\partial\theta}\right)\psi\right]\\
&= Ra_s\frac{1}{r}\frac{\partial}{\partial\theta}(\alpha(z)T - B_1C_1 - B_2C_2 - G\Gamma) \qquad (1)
\end{aligned}$$

Table 1
Model parameters

Parameter	Symbol	Values and units	Non-D value
Rayleigh number	Ra_s	N/A	1.4×10^5
Ave. internal heating	$\langle R(C_1, C_2)\rangle$	9.52×10^{-12} W/kg	25.6
Viscosity prefactor	A	2.4×10^{21} Pa s	0.0024
Dissipation number	Di_0	N/A	1.13
Temperature scale	ΔT	2500 K	1.0
Reference density	ρ_0	3300 kg/m^3	1.0
Ref. expansivity	α_0	5×10^{-5}/K	1.0
Ref. diffusivity	κ_0	7×10^{-7} m^2/s	0.635
Ref. viscosity	η_0	1×10^{24} Pa s	1.0
Heat capacity	c_p	1250 J/(kg K)	1.0
Thickness	d	2890 km	1.0
Velocity	$\boldsymbol{u}$	1 cm/year	1310
Time	t	378 Gyears	1.0
Heat flux	F	2.50 mW/m^2	1.0

$$\left(1+\gamma_c^2 G\frac{\mathrm{d}\Gamma}{\mathrm{d}\pi}DiT\right)\frac{\partial T}{\partial t}+\nabla(\boldsymbol{u}T-\kappa(z)\nabla T) = R(C_1,C_2)+\frac{Di}{Ra_s}\eta(T,z)\dot{e}^2 + \left(1+\gamma_c G\frac{\mathrm{d}\Gamma}{\mathrm{d}\pi}\right)Di\alpha(z)u_r T \quad (2)$$

$$\frac{\partial C_i}{\partial t}+\nabla(\boldsymbol{u}C_i)=0;\quad i=1,2 \quad (3)$$

where ψ is the stream function, T the temperature, C_1 the fraction of P-type material, C_2 the fraction of E-type material, $\eta(T,z)$ the viscosity as a function of temperature and depth, $\dot{e}$ the second invariant strain rate, and $\boldsymbol{u}=(u_r,u_\theta)$ the flow velocity given by:

$$\boldsymbol{u}=(u_r,u_\theta)=\left(\frac{1}{r}\frac{\partial\psi}{\partial\theta},-\frac{\partial\psi}{\partial r}\right) \quad (4)$$

The depth-dependent thermodynamic properties are given by:

$$\alpha(z)=\alpha_0\rho_r(z)^{-n} \quad (5)$$

$$\kappa(z)=\kappa_0\frac{\rho_r^3(z)}{\langle\rho_r(z)\rangle} \quad (6)$$

where z is depth of the mantle calculated from $z=(r_o-r)/(r_o-r_i)$, n the constant where it is here assumed that $n=3$, and the reference density based on thermodynamics constraints is given by:

$$\rho_r(z)=\begin{cases}\rho_0\left(n\dfrac{Di_0}{\gamma_g}z+1\right)^{1/n} & z<z_{660}\\ \Delta\rho_p+\rho_0\left(n\dfrac{Di_0}{\gamma_g}z+1\right)^{1/n} & z\geq z_{660}\end{cases} \quad (7)$$

where $Di_0(=\alpha_0 g d/c_p)$ is the dissipation number defined as surface values of physical properties, the dissipation number at arbitrary depth is given by $Di=Di_0\alpha(z)$ and $\gamma_g=1.091$ is the Gruneisen parameter, values in $\langle\,\rangle$ means a volume average, $\Delta\rho_p$ is the density difference due to an endothermic phase transition. Profiles of each property are shown in Fig. 1(a).

Non-dimensional numbers used in these equations are the Rayleigh number based on the scaled viscosity $Ra_s=\rho_0 g\alpha_0\Delta T(r_o-r_i)^3/\kappa_0\eta_0$, chemical buoyancy ratios for the P-type material; $B_1=\Delta\rho_{c1}/\rho_0\alpha_0\,\Delta T$ and for E-type material; $B_2=\Delta\rho_{c2}/\rho_0\alpha_0\,\Delta T$, the phase buoyancy ratio $G=\Delta\rho_p/\rho_0\alpha_0\,\Delta T$, and the internal heating ratio as a function of chemical compositions given by

$$R(C_1,C_2)=R_0(1-C_1-C_2)+fC_1R_0+gC_2R_0 \quad (8)$$

where f and g are the concentration of internal heating source in the primitive mantle and the dense material in the CMB region, respectively, which these values

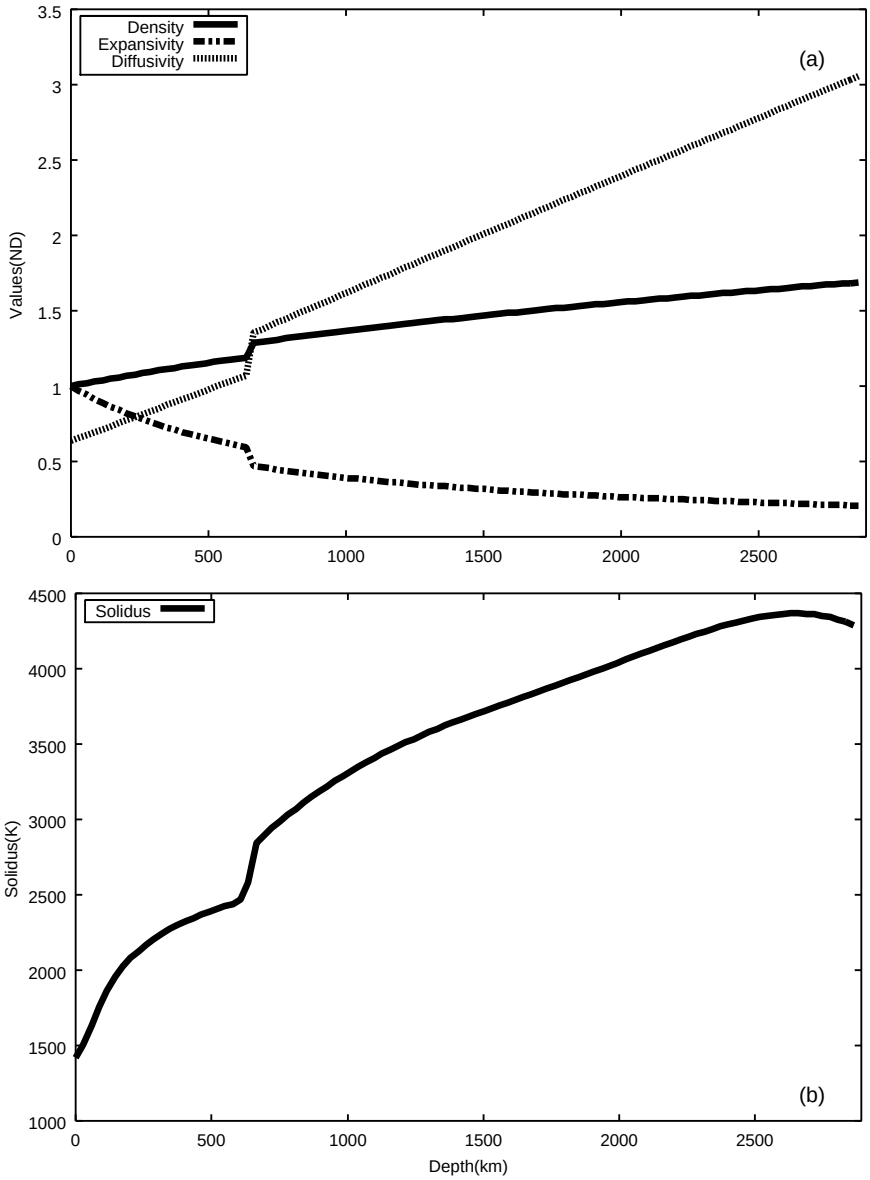

Fig. 1. (a) Profiles of depth-dependent properties of thermodynamic parameters. Solid line: reference density; dashed line: thermal expansivity; dotted line: thermal diffusivity; (b) depth-dependent profile of the melting temperature.

are fixed 5 here, and $R_0 = \rho_0 H(r_o - r_i)^2/k\,\Delta T$ is the internal heating rate in the regular (the depleted MORB) mantle.

The viscosity depends on temperature, depth and composition (E-type material) using a non-dimensionalized form of viscosity similar to Newtonian formulation of Van den Berg and Yuen (1998) given by:

$$\eta(T, z) = AF(z)\exp[-\ln\Delta\eta_c C_2]\exp\left[\frac{g_v T_m(z)}{T_d + T_0}\right] \quad (9)$$

where $A = 2.4 \times 10^{21}$ Pa s is the viscosity prefactor, $\Delta\eta_c$ is the viscosity variation due to E-type material,

$g_v = 5/3$ is the Weertman coefficient, $T_0 = 800\,\mathrm{K}$ is the temperature offset to avoid the extremely viscosity variation in the surface region, T_d is the dimensional temperature, that is calculated as $T_\mathrm{d} = T_\mathrm{s} + T\,\Delta T$, $T_\mathrm{m}(z)$ is the melting temperature of pyrolite composition approximated to be the averaged composition of mantle (Zerr et al., 1998) and plotted in Fig. 1(b), and $F(z)$ is a viscosity jump as a function of depth given by:

$$F(z) = \begin{cases} 30; & z \geq z_{660} \\ 1; & z < z_{660} \end{cases} \tag{10}$$

where z_{660} is the dimensional depth at the position of upper/lower mantle boundary. The non-dimensional viscosity is calculated from the ratio of calculated viscosity to scaled viscosity (10^{24}). The viscosity changes with 100 for temperature and 100 for depth, including in the viscosity jump at the phase boundary, by using these values.

An endothermic phase transition at 660 km is expressed by using the phase function defined by (Christensen and Yuen, 1984; Christensen and Yuen, 1985; Nakakuki et al., 1994). The phase function is given by:

$$\Gamma = \frac{1}{2}\left[1 + \tanh\left(\frac{\pi}{d_\mathrm{ph}}\right)\right] \tag{11}$$

where π is the excess pressure caused by the phase transition written by:

$$\pi = r_\mathrm{ph} - r - \gamma_\mathrm{c} T \tag{12}$$

and d_ph is the half thickness of the phase boundary, γ_c is the non-dimensionalized Clapeyron slope given by $\gamma_\mathrm{c} = \gamma_{\mathrm{c,dim}}\,\Delta T/\rho_0 g d$, and r_ph is the radial position of phase boundary. The derivative of phase function for the excess pressure is calculated to be:

$$\frac{\mathrm{d}\Gamma}{\mathrm{d}\pi} = \frac{2}{d_\mathrm{ph}}(\Gamma - \Gamma^2) \tag{13}$$

We use the modified phase buoyancy ratio that is usually applied to the convection with an endothermic phase transition that is defined as:

$$P = \gamma_\mathrm{c}\frac{\Delta\rho_\mathrm{p}}{\rho_0\alpha_0\,\Delta T} = \gamma_\mathrm{c} G \tag{14}$$

where $\Delta\rho_\mathrm{p}$ is the density difference caused by an endothermic phase transition. The dependence of convective style on this parameter has been already studied by using many models (Christensen and Yuen, 1984; Machetel and Weber, 1991; Solheim and Peltier, 1994; Tackley et al., 1994; Nakakuki et al., 1994; Yuen et al., 1994). The Clapeyron slope at 660 km has been determined to have a negative value from the high pressure experiments (e.g., Ito and Takahashi, 1989; Ito et al., 1990). Here, it is assumed that $\gamma_\mathrm{c} = -0.1$, which corresponds to a dimensional Clapeyron slope of $-3.8\,\mathrm{MPa/K}$. While this is larger than the presently-preferred experimental value of $\sim -2.5\,\mathrm{MPa/K}$, the effect of the phase transition is strongly dependent on the convective vigor commonly expressed in terms of an effective Rayleigh number (Christensen and Yuen, 1985), so this higher-than-realistic value is intended to compensate for the lower-than realistic Rayleigh number of the presented cases. The value of G is given by $G = 0.72$ corresponding to $P = -0.072$. The top and bottom boundaries are impermeable, free slip, and isothermal ($T_\mathrm{s} = 0$; 300 K and $T_\mathrm{cmb} = 1.48$; 4000 K). Side boundaries are periodic.

A finite difference method based on the control volume formulation (Patankar, 1980) is applied to solving equations of motion and temperature. The descretized form of the equation of motion is solved by using an LU decomposition scheme (i.e. direct solver for linear equations using LAPACK (http://www.netlib.org/lapack/)) with the general band matrix for coefficient matrix. The temperature equation is solved by using an upwind procedure in the advection term and central differences in the diffusion term, and an Euler explicit scheme for time integration satisfying with the Courant time step condition. For solving the chemical equation, we use a tracer particle approach following a similar procedure to Tackley and King (2003). The numerical grid consists of 64 points in the radial direction and 180 points in the angular direction with eight tracers in each grid to track the chemical composition.

3. Cases and experimental details

Six chemically heterogeneous scenarios are presented in addition to isochemical convection. The scenarios are: with P-type material (small density

Table 2
Summary of runs

No.	$\Delta\eta_c$	B_1	B_2	d_c (km)	v_s (cm/year)	F_s (mW/m^2)	$d\ln V_s$ (%)
IC	1	N/A	N/A	N/A	0.99	66.33	0.29
R1	1	0.15	N/A	1290	1.21	62.80	0.35
R2	1	0.64	N/A	1290	0.54	35.65	0.25
R3	1	N/A	0.64	289	0.71	49.08	0.51
R4	1	0.15	0.64	1290	0.71	52.14	0.40
CV1	10	0.15	0.64	1290	1.01	58.48	Not calculated
CV2	100	0.15	0.64	1290	1.07	58.88	Not calculated

d_c is the initial thickness of compositional anomaly, v_s is the time-averaged surface RMS velocity, and F_s is the time-averaged surface heat flux. For $d\ln V_s$, the values are represented as a maximum amplitude of seismic anomaly at 4.5 Gyears.

difference and large density difference), with E-type material, including both P- and E-type materials (i.e., a three-component system), and three-component system with a composition-dependent viscosity (viscosity variation due to E-type material is chosen to be 10 and 100). The summary of each run is listed in Table 2.

The chemical buoyancy ratios of P- and E-type components are $B_1 = 0.15$ or 0.64 and $B_2 = 0.64$, respectively. The former value is based on the estimate of density difference from seismic tomographic models (Forte and Mitrovica, 2001) and similar to the value that has been discussed in Kellogg et al. (1999), while the latter value must be high enough for the material to form a layer that is stable over billions of years. The used value was arrived at after some experimentation, and corresponds to a density difference of 8%, higher than the estimate of Sleep (1988) of at least 6%.

Initial conditions for the temperature field (Fig. 3(a) and (b)) are statistically steady-state solutions of purely thermal (i.e., isochemical) convection with the lower layer enforced as a fixed and impermeable boundary. For the compositional fields, the E-type component, when present, initially occupies the lowest 289 km (measured from the CMB) of the mantle (roughly the depth of D″), whereas the P-type component initially occupies 1290 km (also measured from the CMB) of the mantle (corresponding to geochemical mass balance estimates of the amount of primitive material) excluding the region occupied by the E-type component when it is present. The time integration has been carried out for 20,000 steps from the initial condition, corresponding to times of 1.9265×10^{-2} (7.29 Gyears).

4. Results

4.1. Time dependence

Fig. 2 shows Nusselt number in the surface boundary as a function of time for all cases. This indicates that most cases have been reached a statistical steady-state in $t = 0.004$–0.006 (1.51–2.27 Gyears dimensional time). Results presented in the following sections might thus be considered to be thermally statistical steady state solutions for thermo-chemical convection.

4.2. Convective structure

Fig. 3(c)–(f) shows temperature and compositional structures after 4.5 Gyears approximately. With only P-type material with a small density difference (Fig. 3(c)), the temperature field indicates a whole mantle convection, which is composed of large scale of upwelling plume reaching the surface and two cold downwellings subducting to the CMB. Most of the P-type material has been entrained by upwelling plumes from the CMB and forms two huge blobs.

Fig. 3(d) shows temperature and compositional structures for the case with P-type material that has a large density difference. The compositional stratification can be preserved for 4.5 Gyears because the density difference is too large for the much of dense material to be entrained.

Fig. 3(e) shows temperature and compositional structures for the case with only a thin layer of the E-type material. For the temperature field, small-scale convection is dominant in the upper mantle, whereas large-scale convection is dominant in the lower man-

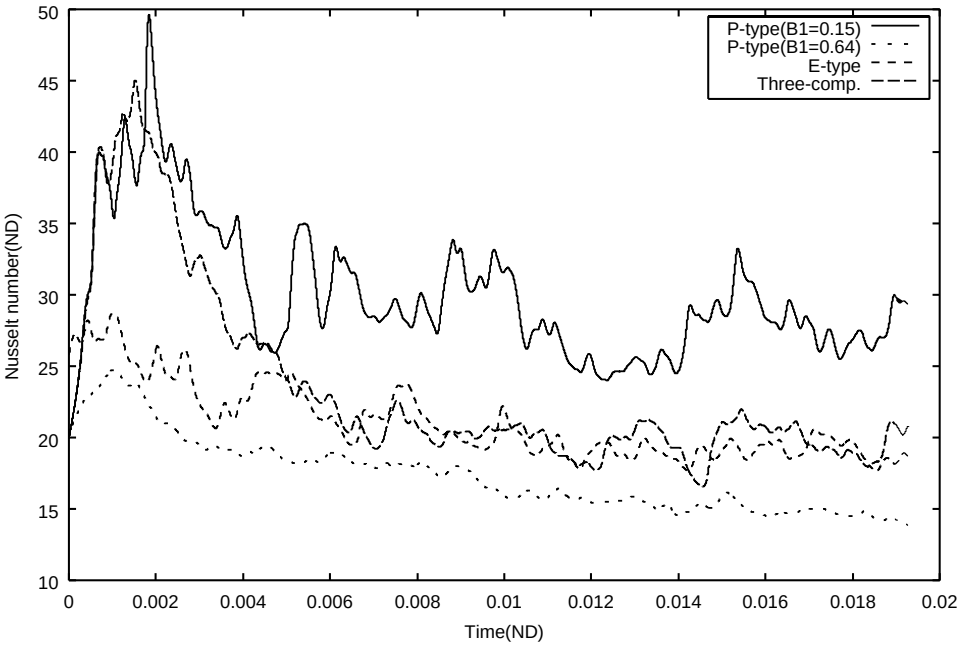

Fig. 2. The surface Nusselt number as a function of time.

tle. Upwelling plumes are trapped at the phase boundary, and small-scale upwelling plumes in the upper mantle (red arrowed in Fig. 3(e)) forms hot material pooling below the 660 km boundary. Those plumes are generated by a completely thermal origin. The dense material has been swept into two isolated piles, from which two upwelling plumes rise, entraining a small amount of dense material. These plumes are generated by the combination of two heat sources; dense material enriched in the heat-generating elements and heat from the core.

Fig. 3(f) shows temperature and compositional fields for the case of the three component system, which shows a mixture of features from the former two cases. The temperature structure becomes a partially-layering with two scales of upwelling plumes: from the CMB region and from the phase boundary. The E-type material forms isolated piles from which large-scale upwelling plumes rise. The P-type material is dispersed by the convective flow, and forms the blob structures. Small-scale upwelling plumes might be generated from blob structures (red arrowed in Fig. 3(f)) weakly trapped at the phase boundary (by the filtering effect for dense material (Weinstein, 1992)) because of enhancement of heat-producing elements in the P-type material by a similar mechanism described for the case with only E-type material.

To compare the convective vigor to the present Earth, it is useful to consider the time-averaged surface velocity and heat flux shown in Table 2. For the surface velocity, it range from 0.54 to 1.20 cm per year in case of compositional anomaly and becomes 0.99 cm per year in case of isochemical convection. These are half to one orders of magnitude lower than the Earth's present plate velocities. The surface heat flux in these models is ranged from 35.65 mW/m^2 (P-type material with a large density difference) to 62.80 mW/m^2 (P-type with a small density difference). Comparing to Earth, these values are from a factor of two to slightly lower than the present heat flux (approximately 75 mW/m^2 (Pollack et al., 1993)).

4.3. Viscosity structure

Fig. 4 shows the radial viscosity structure for chemically-heterogeneous cases. The viscosity in the upper mantle is almost similar profiles to each case.

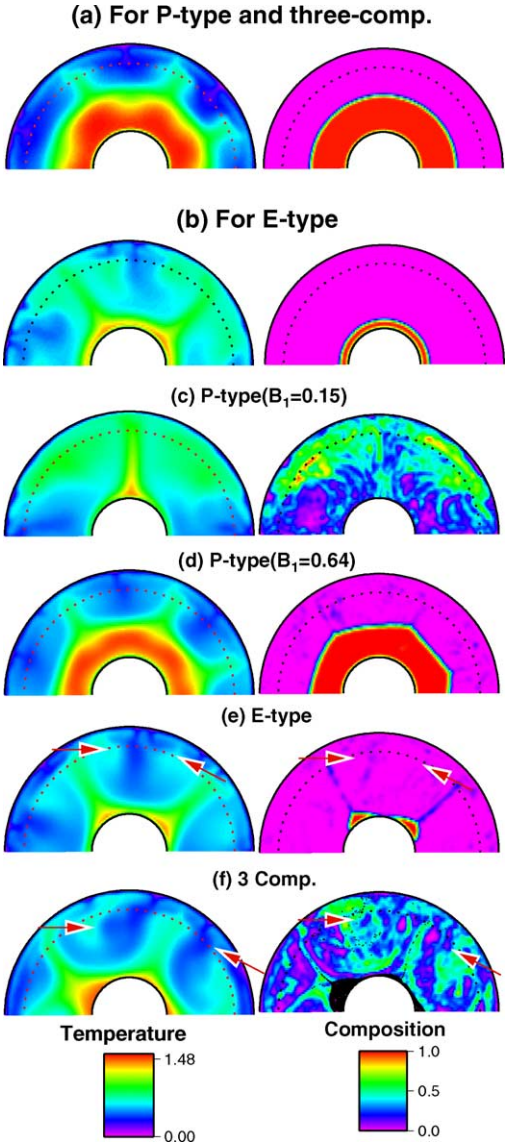

Fig. 3. Temperature (left) and compositional field (right). Initial condition for: (a) P-type material and three-component system and (b) E-type material. P-type material: (c) ($B_1 = 0.15$) and (d) ($B_1 = 0.64$). (e) E-type material only; (f) three-component. Red arrows in (e) and (f) shows small-scale plumes from near phase boundary. The color bars show non-dimensional values of temperature and composition. The black dots in (f) show the tracer particle of E-type material. Red dotted line in the temperature and residual temperature field and black dotted line in the compositional field are shown as the phase boundary.

The viscosity in the lower mantle is different among these cases. The three-component system and only E-type is almost the same viscosity profiles. For the P-type material, the viscosity profiles obtained in a small density difference is approximately factor of two lower than for three-component system and E-type material because the dense P-type material can be distributed in the whole mantle and the effect of temperature dependent viscosity. On the other hand, for the P-type material with a large density difference, the viscosity is rapidly decreased at the compositional boundary because the dense material is enhanced by heat-producing elements and the viscosity is dependent on the temperature.

4.4. Seismic structure

In order to compare the structures in the results to those in Earth's mantle, it is most useful to consider the seismic velocity signature, as this is imaged by global tomography. Here the seismic structure is given as a function of temperature and the iron contents X_{Fe} converted from the compositional field:

$$
\begin{aligned}
d\ln V_{\mathrm{s}} &= \frac{\partial \ln V_{\mathrm{s}}}{\partial T}\delta T + \frac{\partial \ln V_{\mathrm{s}}}{\partial X_{\mathrm{Fe}}}\delta X_{\mathrm{Fe}} \\
\frac{\partial \ln V_{\mathrm{s}}}{\partial T} &= a_{T1} + a_{T2}z + a_{T3}z^2 \\
\frac{\partial \ln V_{\mathrm{s}}}{\partial X_{\mathrm{Fe}}} &= a_{C1} + a_{C2}z + a_{C3}z^2 \\
X_{\mathrm{Fe}} &= X^0_{\mathrm{Fe}} + \Delta X_{\mathrm{Fe}}(C_1 + C_2)
\end{aligned}
\tag{15}
$$

where partial derivatives for temperature and compositional fields are dependent on the depth, coefficients are given by Trampert et al. (2001), $X^0_{\mathrm{Fe}} = 0.05$ is the iron contents in the regular mantle, and $\Delta X_{\mathrm{Fe}} = 0.1$ is the range of variation in iron contents due to the compositional field. The iron content X_{Fe} ranges from 0.05 to 0.15. Fig. 5 shows the seismic anomalies structure for four cases. With only P-type material (Fig. 5(a)), which has a small density contrast, no large seismic anomalies are observed at the base of the mantle except for upwelling regions, and low velocity regions form blob-like structures throughout the mantle. For only P-type material having a large density contrast (Fig. 5(b)), a relatively small contrast of seismic velocity can be observed in the compositional boundary (1600 km depth). With only E-type material, or with

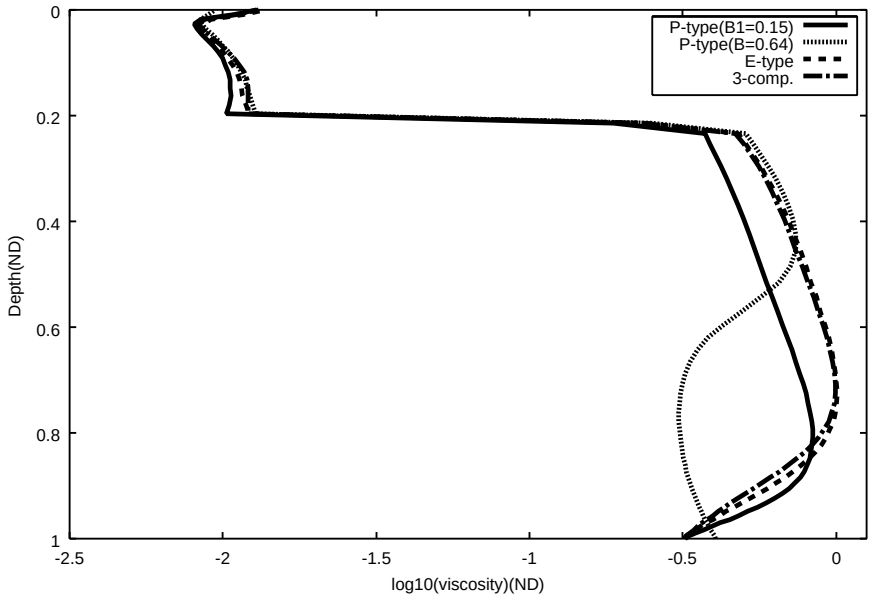

Fig. 4. The radial profiles of viscosity for chemically-heterogeneous cases.

all components (Fig. 5(c) and (d), respectively), a large contrast in seismic anomaly is observed at the base of the mantle is observed, and the most pronounced low velocity regions correspond to upwelling plumes found in Fig. 3(e) and (f).

Fig. 6 shows power spectra of seismic structure versus depth along with the depth profile or rms power, calculated using above conversions to seismic velocity (Eq. (15)), and considering either temperature alone, or the combined effect of temperature and composition.

For isochemical convection (Fig. 6(a)), temperature-based seismic anomalies are dominated by degree of two, in surface and CMB region. These two signatures are generated as instabilities of thermal boundary layers. The rms profile of seismic anomaly is approx-

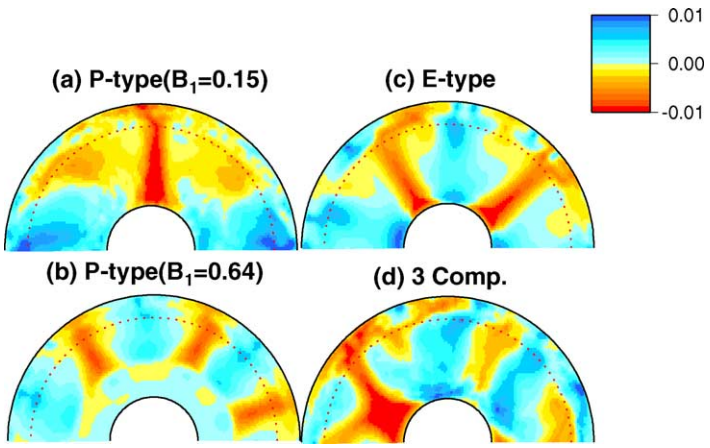

Fig. 5. Seismic anomaly calculated from Fig. 3. P-type material: (a) ($B_1 = 0.15$) and (b) ($B_1 = 0.64$). (c) E-type material. (d) Three-component. The color bar shows that the red is low velocity anomaly and blue is high velocity anomaly ($\times 100\%$).

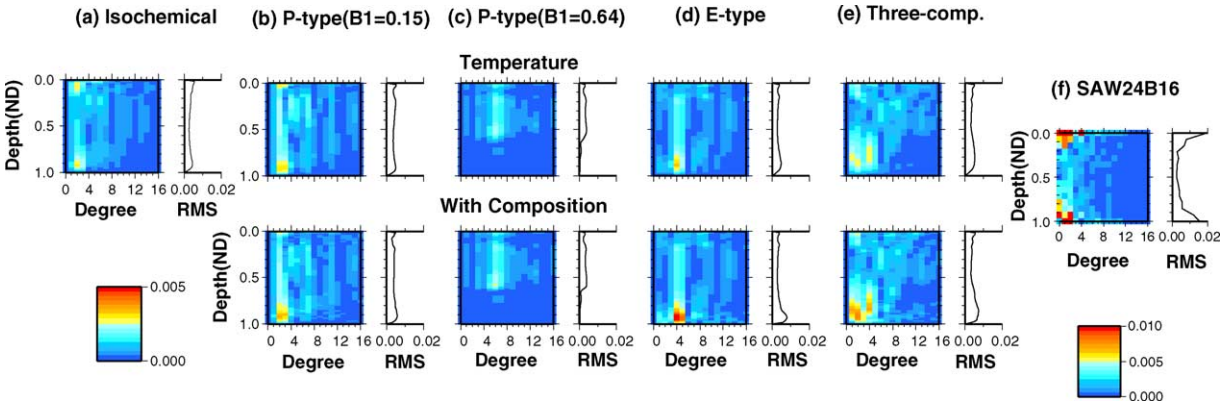

Fig. 6. Spectrum heterogeneity map (left) and rms profile (right) calculated from Fig. 4. (a) Isochemical. P-type material: (b) ($B_1 = 0.15$) and (c) ($B_1 = 0.64$). (d) E-type material. (e) Three-component. (f) Global tomography model (Megnin and Romanowicz, 2000). The unit for color bars is shown as $\times 100\%$.

imately 0.3% in the boundary region (surface and CMB; see Table 2). With small density contrast P-type material (Fig. 6(b)), two strong signatures, which are dominated by the degree of two and caused by the instabilities of thermal boundary layers at the surface and CMB, and one signature are observed when only temperature is considered, but when composition is included, a strong signature in the upper mantle similar to the isochemical case. The peak value of the rms profile is still 0.35% in surface and CMB region (see Table 2). For large density contrast P-type material (Fig. 6(c)), the signature beneath the compositional boundary is almost zero and a weak signature corresponding to the topography of the compositional boundary is found at the depth of 1600 km. The rms values of seismic anomalies slightly increases when chemical composition is included. The maximum amplitude of seismic anomaly is estimated to be 0.25% when the compositional anomaly is included. With a thin, E-type layer that forms one large pile (Fig. 6(d)), the temperature-based anomalies do not have a strong signature in the whole mantle but there is a slightly strong signature, which is dominated by degree of four corresponding to two isolated piles, in the CMB region. However, composition generates larger heterogeneity amplitudes in the deepest mantle. The maximum amplitude of seismic anomaly is estimated to be 0.51%, which is approximately a factor of two larger than in cases of only P-type material (Table 2). With all components present (Fig. 6(e)), a low degree structure is dominant at the base of the mantle if only the temperature effect is considered, and considering composition adds large amplitude, long-wavelength heterogeneity near the CMB (where the stable compositional 'piles' exist). A "red" spectrum can be found only near the CMB.

4.5. Comparison with the global tomography model

Fig. 6(f) shows the spectral decomposition and rms profile of seismic anomalies for global tomography model SAW24B16 (Megnin and Romanowicz, 2000). The spectral map (left of Fig. 6(f)) can be compared to numerical results. The main features of the spectral heterogeneity map of the global tomographic model are a strong "red" spectrum in the CMB region and surface, and lower amplitude, broader (less red) spectrum in the mid-mantle. The rms profiles (right of Fig. 6(f)) can also be compared to numerical results. The rms profiles on global tomography model are large values (approximately 1% of seismic anomaly) in the surface and CMB region. The numerical results that are the closest to tomography models in their spectra are those of the three-component system (Fig. 5(e)) for the dominant degree of seismic anomaly and the E-type material case for the amplitude. Note that spectra profiles obtained from other tomography models (e.g., Becker and Boschi, 2002; Gu et al., 2001) show a similar distribution to that presented here (Megnin and

Romanowicz, 2000), and support the current arguments. Note that many of global tomography model have a lot of problems in their models, which is related to the resolution in the CMB region, since the coverage of ray-path in the CMB region is not enough to resolve the fine structure. However, our target is understanding the large-scale structure in the CMB region, most tomography models could obtain the similar structure for lower degree structure, thus, the comparison in this paper may be reasonable for understanding the seismic structure in the CMB region.

4.6. Composition-dependent viscosity

Fig. 7 shows temperature and compositional fields for including the composition-dependent viscosity. The temperature in the CMB region is slightly hotter than without the composition-dependent viscosity (Fig. 3(f)). For 10 times viscosity variation due to E-type material, there are two isolated piles in the CMB region. On the other hand, for 100 times viscosity variation, one large isolated pile can be found in the CMB region. This implies that the composition-dependent viscosity can be expected to be more stable layering in the CMB region. The surface heat flux and surface velocity obtained in these two cases are slightly higher than the case without composition-dependent viscosity but lower than the present Earth's values.

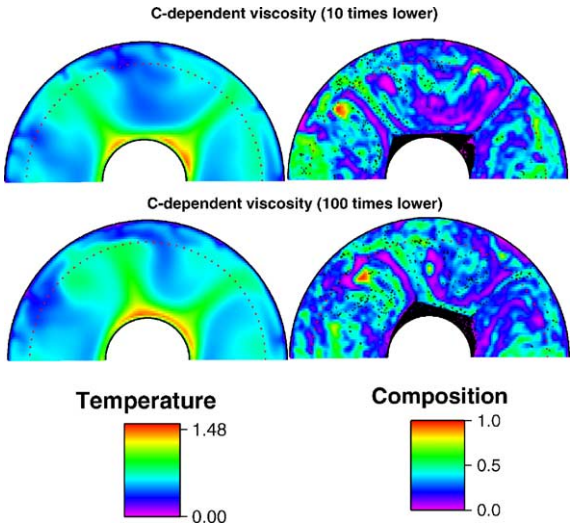

Fig. 7. Temperature (left) and compositional field (right) for adding the composition-dependent viscosity in a three-component system.

Previous studies concerned with the composition-dependent viscosity have been shown by using both laboratory and numerical experiments. The laboratory experiments (Davaille, 1999) concerned with the stability of thin chemical layering in the CMB region have shown in three-dimensional geometry, and found that the chemical layering in the CMB region could be stable in case of smaller density variation in that region when it would be less viscous than the regular mantle. The numerical experiments (Schott et al., 2002) have shown the importance of composition-dependent viscosity and compressibility of the mantle, which can be expected to be more stable layering in the CMB region compared to Boussinesq and without composition-dependent viscosity. However, it is not clear how large the composition-dependent viscosity is discussed by the aspect of the mantle rheology since the chemically-dense material may gets hot due to an enhanced heat-producing elements and is likely to be less viscous. For example, in case of no composition-dependent viscosity, the viscosity variation due to an enhanced heat-producing elements can be estimated as three times less viscous than the regular lower mantle (see Fig. 4).

5. Discussion

5.1. Convective mixing

It is clear that material with a chemical buoyancy contrast as low as the 1–2% inferred by Forte and Mitrovica (2001) from considerations of seismic tomography, cannot remain as a stable layer but will be dispersed by the convection throughout the mantle, although the effect of their inferred mid-mantle viscosity maximum is not tested here. This result suggests that it seems difficult to keep primitive material out the MORB source region (i.e., shallow mantle) using this mechanism. This needs to be carefully examined using a more realistic mineralogical model.

Although the P-type material is widely dispersed, it has not become well stirred even after the 4.5 Gyears modeled time, contrary to expectations from mixing studies (Christensen, 1989; Kellogg and Turcotte, 1991). One explanation is that the convective veloci-

ties in these calculations are lower than Earth-like by a factor of 5–10, based the comparison of surface velocities made earlier, in which case the modeled time may more reasonably correspond to a dimensional time of only 450–900 Myears. Even so, the stretching rate seems slow slightly, and this warrents further investigation.

5.2. Seismic anomaly in the CMB region and hybrid plumes model

Ritsema et al. (1998) and Ni et al. (2002) pointed out the existence of sharp boundary of seismic anomalies in the CMB region below Africa, where the large-scale upwelling plume has been seismically observed, and they suggested that such a boundary can be obtained from the thermo-chemical anomalies in the CMB. When including the dense and E-type material in our study, seismic anomalies in the CMB have sharp boundaries. The velocity jump in such boundaries is expected to be several percents from the observed seismic anomalies; in the presented results it is as at least 1%.

Zhao (2001) pointed out the existence of small-scale upwelling flow from just below the transition zone in a global tomography model, in addition to large-scale upwelling plumes from the CMB region. The excess temperature of such plumes was estimated to range from 100 to 300 K based on the observed velocity structures. In the models presented here, such small-scale plumes can be generated as purely thermal effects detached from upwelling plumes above the CMB or by enhanced heat production in the upper part of the lower mantle caused by accumulation of enriched material (see Fig. 3(e) and (f)). The excess temperature of small-scale plumes above the phase boundary in the present models is 250 to 500 K, but this needs to be more accurately determined using more realistic models including three dimensionality.

5.3. Uncertainty in converting temperature and composition to seismic anomalies

In order to obtain the seismic anomalies from our simulation results, the simple relationship (see Eq. (15)) derived from the mineral physics has been used here. There is a problem about the coefficients using a conversion from temperature and composition fields to seismic anomalies. Trampert et al. (2001) has showed that there is strongly uncertainty in converting the compositional anomalies to seismic anomalies, which is several 10's of percent of discrepancy in determining the coefficients for calculating such relationship. It is necessary for determining the coefficients for converting the temperature and compositional fields to seismic anomalies to determine the chemical composition of the lower mantle precisely. However, this uncertainty may affect with the amplitude of seismic anomalies, there is no influence to the characteristic degree of seismic anomalies because the scale of seismic anomalies may correspond to the characteristic scale of density field which is combined between temperature and chemical composition.

5.4. Geochemical geodynamics

According to geochemical constraints on chemical recycling in the mantle convection system, each chemically-distinct recycled component has a different residence time (e.g., Albarede, 1998), which may be inconsistent with a simple whole-mantle convection model. For example, while Christensen and Hoffmann (1994) were able to obtain the correct residence time to generate the HIMU-MORB trend by segregating subducted crust above the CMB, other components with different residence times require different mechanism(s). The hybrid plumes model obtained in this study, in which some plumes come from above the CMB but some come from the top of the lower mantle, may be a way of generating multiple residence times as well as sampling different chemical components or 'reservoirs', as observed in OIBs, although this needs to be quantified.

5.5. Influences of higher Rayleigh number

The Rayleigh number also affects with the convective mixing. In this study, the Rayleigh number is not so high compared to the realistic value. If the Rayleigh number would be as high as the realistic Rayleigh number (around 10^7) (Christensen and Yuen, 1985), the convective structure might be resembled as two-layered convection and the compositional anomaly could be stayed in the lower mantle,

which means the filtering effect at the phase boundary becomes much stronger than the presented results. Therefore, the more clear structure of small scale plumes from the phase boundary might be expected in case of higher Rayleigh number. The influences to the seismic structure in that case might not be so changed.

6. Conclusions

Conclusions are as follows.

1. Strong heterogeneity at the base of the mantle observed in global seismic tomography models can be generated by compositional anomalies in the CMB region.
2. A plausible compositional structure in the convecting mantle is that the primitive material forms the blob structure spread out in the whole mantle, with isolated "piles" of recycled material in the CMB region. This indicates that two distinct geochemical reservoirs, which one is semi-stable layer (isolated piles) in the CMB region producing the HIMU type OIB and another is widely dispersed in the lower mantle producing other types of OIBs, are necessary for understanding both geochemical and seismological constraints.
3. Two types of hybrid plumes, one fed by hot material just below the 660 km discontinuity, and one rising from chemically-dense piles above the CMB, may coexist. This model may be consistent with geochemical constraints for the residence time of isotope analysis. The presented results are not completely Earth-like because the convective vigor is lower than realistic values and the geometry used here is not three-dimensional. The further investigations will be necessary for the problems of realistic rheology and geometry.

Acknowledgements

Authors thank H. Iwamori and T. Nakakuki for constructive comments and discussions, and Dave Yuen and Bertram Schott for helpful review to improve the manuscript. T.N. was financially supported by JSPS Research fellowship for young scientists and by the David and Lucile Packard Foundation. S. Xie helped for making Fig. 1(b).

References

Albarede, F., 1998. Time-dependent models of U–Th–He and K–Ar evolution and the layering of mantle convection. Chem. Geol. 145, 413–429.

Albarede, F., van der Hilst, R.D., 1999. New mantle convection model reconcile conflicting evidence. EOS 45, 535–539.

Becker, Th.W., Kellogg, J.B., O'Connell, R.J., 1999. Thermal constraint on the survival of primitive blobs in the lower mantle. Earth Planet. Sci. Lett. 171, 351–365.

Becker, Th.W., Boschi, L., 2002. A comparison of tomographic and geodynamic mantle models. Geochem. Geophys. Geosyst. 3, Paper number 2001GC000168.

Christensen, U.R., Yuen, D.A., 1984. The interaction of a subducting slab with a chemical and phase boundary. J. Geophys. Res. 89, 4392–4402.

Christensen, U.R., Yuen, D.A., 1985. Layered convection induced by phase transitions. J. Geophys. Res. 90, 10291–10300.

Christensen, U.R., 1989. Mixing by convection in mantle. Earth Planet. Sci. Lett. 95, 382–394.

Christensen, U.R., Hoffmann, A.W., 1994. Segregation of subducted oceanic crust in the convecting mantle. J. Geophys. Res. 99, 19867–19884.

Cotice, N., Ricard, Y., 1999. Geochemical observation and one layer mantle convection. Earth Planet. Sci. Lett. 174, 125–137.

Davaille, A., 1999. Simultaneous generation of hotspots and superswells by convection in a heterogeneous planetary mantle. Nature 402, 756–760.

Ferrachat, S., Ricard, Y., 2001. Mixing properties in the Earth's mantle: effects of the viscosity stratification and of oceanic crust segregation. Geochem. Geophys. Geosyst. 2, Paper number 2000GC000092.

Forte, A.M., Mitrovica, J.X., 2001. Deep-mantle high viscosity flow and thermochemical structure inferred from seismic and geodynamics data. Nature 410, 1049–1056.

Gu, Y.J., Dziewonski, A.M., Su, W., Ekstrom, G., 2001. Models of the mantle shear velocity and discontinuities in the pattern of lateral heterogeneities. J. Geophys. Res. 106, 11169–11199.

Hofmann, A.W., 1997. Mantle geochemistry: the message from oceanic volcanism. Nature 385, 219–229.

Ishii, M., Tromp, J., 1999. Normal-mode and free-air gravity constraints on lateral variation in velocity and density of Earth's mantle. Science 285, 1231–1235.

Ishii, M., Tromp, J., 2001. Even-degree lateral variations in the Earth's mantle constrained by free oscillations and the free-air gravity anomaly. Geophys. J. Int. 145, 77–96.

Ito, E., Takahashi, E., 1989. Postspinel transformation in the system Mg_2SiO_4–Fe_2SiO_4 and some geophysical implication. J. Geophys. Res. 94, 10637–10646.

Ito, E., Akaogi, M., Toper, L., Navrotsky, A., 1990. Negative pressure–temperature slopes for reactions forming Mg_2SiO_3 perovskite from carimety. Science 249, 1275–1278.

Karato, S., Karki, B.B., 2001. Origin of lateral variation of seismic wave velocities and density in the deep mantle. J. Geophys. Res. 106, 21771–21784.

Kellogg, L.H., Turcotte, D.L., 1991. Mixing and the distribution of heterogeneities in a chaotically convective mantle. J. Geophys. Res. 95, 421–432.

Kellogg, L.H., van der Hilst, R.D., Hager, B.H., 1999. Compositional stratification in the deep mantle. Science 283, 1881–1884.

Lay, T., Williams, Q., Garnero, E.J., 1998. The core–mantle boundary layer and deep Earth dynamics. Nature 392, 461–468.

Machetel, P., Weber, P., 1991. Intermittent layered convection in a model mantle with an endothermic phase transition at 670 km. Nature 350, 55–57.

Manga, M., 1996. Mixing of heterogeneities in the mantle: effect of viscosity difference. Geophys. Res. Lett. 23, 403–406.

McNamara, A.K., van Keken, P.E., 2000. Cooling of the Earth: a parameterized convection study of whole versus layered models. Geochem. Geophys. Geosyst. 1, Paper number 2001GC000045.

Megnin, C., Romanowicz, B.A., 2000. The 3D shear velocity structure of the mantle from the inversion of body, surface and higher mode waveforms. Geophys. J. Int. 143, 709–728.

Meriaux, C., Agnon, A., Lister, J.R., 1998. The thermal signature of subducted lithospheric slabs at the core–mantle boundary. Earth Planet. Sci. Lett. 160, 551–562.

Nakakuki, T., Sato, H., Fujimoto, H., 1994. Interaction of the up welling plume with the phase and chemical boundary at the 670 km discontinuity: effects of temperature dependent viscosity. Earth Planet. Sci. Lett. 121, 369–384.

Ni, S., Tan, E., Gurnis, M., Helmburger, D.V., 2002. Sharp sides to the African superplume. Science 296, 1850–1853.

Ohtani, E., Maeda, M., 2001. Density of basaltic melt at high pressure and stability of the melt at the base of the lower mantle. Earth Planet. Sci. Lett. 193, 69–75.

Patankar, S.V., 1980. Numerical Heat Transfer and Fluid Flow, Hemisphere.

Pollack, H.N., Hunter, S.J., Johnston, R., 1993. Heat loss from the Earth's interior: analysis of the global data set. Rev. Geophys. 31, 267–280.

Ritsema, J., Ni, S., Helmberger, D.V., Crotwell, H.P., 1998. Evidence for strong shear velocity reductions and velocity gradients in the lower mantle beneath Africa. Geophys. Res. Lett. 25, 4245–4248.

Schott, B., Yuen, D.A., Braun, A., 2002. The influence of composition- and temperature-dependent rheology in thermo-chemical convection on entrainment of the D″-layer. Phys. Earth Planet. Int. 129, 43–65.

Sidorin, I., Gurnis, M., 1998. Geodynamically consistent seismic velocity predictions at the base of mantle. In: Gurnis, M., Wysession, M.E., Knittle, E., Buffet, B.A. (Eds.), The Core–mantle Boundary region. American Geophysical Union, Washington, DC, pp 209–230.

Sleep, N.H., 1988. Gradual entrainment of a chemical layer at the base of mantle by overlying convection. Geophys. J. Int. 95, 437–448.

Solheim, L.P., Peltier, W.R., 1994. Avalanche effects in phase transition modulated thermal convection: a model of the Earth's mantle. J. Geophys. Res. 99, 6997–7018.

Stevenson, D.J., 1990. Fluid dynamics of the core formation. In: Newsom, H.E., Jones, J.E. (Eds.), The Origin of the Earth. Oxford University Press, New York, pp. 231–250.

Trampert, J., Vacher, P., Vlaar, N., 2001. Sensitivities of seismic velocities to temperature, pressure and composition in the lower mantle. Phys. Earth Planet. Int. 124, 255–267.

Tackley, P.J., Stevenson, D.J., Glatzmainer, G.A., Schubert, G., 1994. Effects of multiple phase transition in a three-dimensional spherical model of convection in Earth's mantle. J. Geophys. Res. 99, 15877–15901.

Tackley, P.J., 1998. Three dimensional simulation of mantle convection with a thermo-chemical boundary layer: D″? In: Gurnis, M., Wysession, M.E., Knittle, E., Buffet, B.A. (Eds.), The Core–mantle Boundary Region. American Geophysical Union, Washington, DC, pp. 231–253.

Tackley, P.J., 2000. Mantle convection and Plate tectonics: towards and integrated physical and chemical theory. Science 288, 2002–2007.

Tackley, P.J., 2002. The strong heterogeneity caused by deep mantle layering. Geochem. Geophys. Geosyst. 3, paper number 2001GC000167.

Tackley P.J., King, S.D., 2003. Testing the tracer ratio method for modeling active compositional fields in mantle convection simulations. Geochem. Geophys. Geosyst. 4, paper number 2001GC000214.

Van den Berg, A.E., Yuen, D.A., 1998. Modelling planetary dynamics by using the temperature at the core–mantle boundary as a control variable: effects of rheological layering on mantle heat transport. Phys. Earth. Planet. Int. 108, 219–234.

Van der Hilst, R.D., Karason, H., 1999. Compositional heterogeneity in the bottom 1000 km of Earth's mantle: towards a hybrid convection model. Science 283, 1885–1888.

Van Keken, P.E., 2001. Cylindrical scaling for dynamical cooling models of the Earth. Phys. Earth Planet. Int. 124, 119–130.

Vidale, J.E., Schubert, G., Earle, P.S., 2001. Unsuccessful initial search for a midmantle chemical boundary layer with seismic arrays. Geophys. Res. Lett. 28, 859–862.

Weinstein, S.A., 1992. Induced compositional layering in a convecting fluid layer by an endothermic phase transition. Earth Planet. Sci. Lett. 113, 23–39.

Yuen, D.A., Reuteler, D.M., Balachander, S., Steinbach, V., Malevsky, A.V., Smedsmo, J.L., 1994. Various influence on three-dimensional mantle convection with phase transitions. Phys. Earth. Planet. Int. 86, 185–203.

Zerr, A., Diegeler, A., Boehler, R., 1998. Solidus of Earth's deep mantle. Science 281, 243–246.

Zhao, D., 2001. Seismic structure and origin of hotspots and mantle plumes. Earth Planet. Sci. Lett. 192, 251–265.